Unsteady DMD-based flowfield estimation from embedded pressure sensors in an actuated airfoil

Daniel F. Gomez,*, Phillip B. Kirk†, Andrew H. Lind‡, Anya R. Jones§, and Derek A. Paley ¶
University of Maryland, College Park, MD, 20740

Francis D. Lagor‖
University at Buffalo, The State University of New York, Buffalo, NY, 14260

This paper describes the application of a principled estimation method that generates full flowfield estimates using data obtained from a limited number of pressure sensors on an actuated airfoil, based on Dynamic Mode Decomposition (DMD). DMD is a data-driven algorithm that approximates a time series of data as a sum of modes that evolve linearly. DMD is used here to create a linear system that approximates the flow dynamics and pressure sensor output from Particle Image Velocimetry (PIV) and pressure measurements of the flowfield around the airfoil. Sparsity Promoting DMD (SPDMD) selects a reduced number of modes in order to simplify the system while providing a sufficiently accurate approximation of the flowfield. A DMD Kalman Filter (DMD-KF) uses the pressure measurements to estimate the evolution of this linear system, and thus produce an approximation of the flowfield from the pressure data alone. The DMD-KF is implemented for experimental data from two different setups: a pitching cambered ellipse airfoil and a surging NACA 0012 airfoil. Filter performance is evaluated using the original flowfield PIV data, and compared with a DMD reconstruction.

Nomenclature

DMD	Dynamic Mode Decomposition
SPDMD	Sparsity Promoting DMD
POD	Principal Orthogonal Decomposition
SVD	Singular Value Decomposition
PIV	Particle Image Velocimetry
$\boldsymbol{\psi}(t)$	Vector of observables at time t
$\Psi,\ \Psi'$	Matrices of data snapshots
m	Number of snapshot pairs in original data
n	Dimension of $\boldsymbol{\psi}$
A	Approximate time evolution operator for $\boldsymbol{\psi}$
$\tilde{A}$	SVD projection of A
$U\Sigma V^*$	SVD of Ψ
$\boldsymbol{\phi}_i$	ith DMD eigenmode
Φ	Matrix of DMD eigenmodes
λ_i	ith DMD eigenvalue
Λ	Diagonal matrix of DMD eigenvalues
$\boldsymbol{\alpha}$	Vector of DMD mode amplitudes
γ	SPDMD parameter
J_γ	SPDMD cost function
m^*	Number of modes chosen for reduced-order model

*Graduate Research Assistant, Aerospace Engineering, AIAA student member
†Graduate Research Assistant, Aerospace Engineering
‡Assistant Research Engineer, Aerospace Engineering, AIAA member
§Associate Professor, Aerospace Engineering, AIAA Associate Fellow
¶Willis H. Young Jr. Professor of Aerospace Engineering Education, Aerospace Engineering, AIAA Associate Fellow
‖Assistant Professor, Mechanical and Aerospace Engineering, AIAA member

$\boldsymbol{x}$	Vector of states
$\boldsymbol{y}$	Vector of measurements
$\boldsymbol{z}$	Vector of mode amplitudes in modal form
F	State transition matrix for $\boldsymbol{z}$ dynamics
C_y	$\boldsymbol{y}$ observer matrix
C_x	$\boldsymbol{x}$ observer matrix
$\hat{\boldsymbol{z}}$	Estimate of $\boldsymbol{z}$
P	Estimate covariance
Q	Process noise covariance
R	Measurement noise covariance
K	Kalman gain
t^*	Time, normalized by period of actuation
Amp	Normalized surging amplitude
k	Reduced frequency of actuation

I. Introduction

Unsteady flow structures play an important role in the generation of lift at high angles of attack [1]. For example, during dynamic stall, the lift coefficient increases beyond its value found in the static stall condition, due to the formation of a leading edge vortex (LEV). As the angle of attack increases further, the LEV sheds and the lift coefficient falls [2]. To avoid large, undesirable variations in lift, feedback control may be applied to enhance or regularize unsteady lift production. A prerequisite for feedback control based on flow dynamics is estimation of the flowfield. Estimation can be achieved by a dynamic observer operating on a model of the flowfield. Common approaches include linearization of the Navier-Stokes equations [3], fitting a reduced-order model to experimental data, such as the Goman-Khrabrov model [1], or using modal decompositions [4].

Modal decomposition methods extract a small number of modes that contain most of the information of a set of high-dimensional data. For example, Proper Orthogonal Decomposition (POD) [5] provides a set orthogonal modes that minimize the difference (in the least-squares sense) between the original data and its projection onto the span of modes. While POD modes optimally reproduce the original dataset, they do not necessarily correspond to coherent structures in the flow, nor do they contain any information about the time evolution of the flow [5]. Balanced POD (BPOD) [6] finds modes that are the most controllable and observable, making it very useful for feedback control as in [7]. However, computing BPOD requires prior knowledge of the dynamics of the system.

An alternative modal decomposition that focuses on describing the time evolution is Dynamic Mode Decomposition (DMD). DMD is a data-driven algorithm initially developed for modal decomposition and analysis of fluid flows [8]. In the context of fluid mechanics, DMD decomposes the flow into modes of oscillation and, thus, provides a useful dynamical description of the system. DMD has been commonly used to analyze the behavior of unsteady flow [4]. The traditional procedure used for analyzing a flow using DMD is to assimilate velocity data obtained either computationally or through Particle Image Velocimetry (PIV). Modal decomposition generates a reduced-order, approximate model in terms of the DMD modes, which may be used for estimation.

If DMD is performed with both state and output data, a linear system that approximates the dynamics and the output equation can be constructed, and a Kalman Filter (KF) may be applied to estimate the states [9]. We refer to this filter as a DMD Kalman Filter (DMD-KF). To be useful for estimation, the DMD modes found should not only represent the dataset in which DMD was performed, but also the ensemble of flow trajectories from which the dataset was obtained. Ideally, we wish to obtain modes that are physically significant to the underlying dynamics and, thus, should generalize to different realizations of the same system. DMD may be able to provide such a general model of the dynamics even if the system is nonlinear.

DMD has a close relationship with an operator-theoretic description of dynamical systems based on the Koopman operator [10]. The Koopman operator is an operator that advances observables of a dynamical system linearly in time [11]. It serves as a way to represent a nonlinear system as a linear system [11]. If the DMD modes are able to correctly approximate the Koopman modes of the underlying dynamics, then the DMD-KF is equivalent to the Koopman Kalman

Filter (KKF) [9].

Obtaining physically significant modes is a goal of many DMD related papers: Extended DMD [12] uses a dictionary of functions to better approximate the Koopman operator of the underlying dynamics; Total DMD [13][14] seeks to correct for the effect of noisy data; [5] shows that Spectral POD optimally accounts for the variation in an ensemble of DMD modes; and Sparsity Promoting DMD (SPDMD) [15] finds the most relevant DMD modes for a set of data. Implementing these variations of DMD could potentially improve the perfomance of the DMD-KF, however such an exploration lies beyond the scope of this paper.

This paper applies the DMD-KF to generate full flowfield estimates using DMD modes and data obtained from a limited number of pressure sensors. We define the original data set as the training set, which contains PIV data and pressure measurements. Sparsity Promoting DMD (SPDMD) selects a reduced number of modes in order to simplify the system, while providing a sufficiently accurate approximation of the flowfield. The DMD-KF uses pressure measurements as inputs to estimate a system in which the states are the amplitudes of the DMD modes. With knowledge of the modes and an estimate of the amplitudes, the flowfield is reproduced. We evaluate the performance of the estimator with the original, training data set, and a test data set consisting of a different realization of the same system. Although our analysis was conducted offline, the estimator may be useful for real-time analysis and control of the flowfield when in-situ PIV measurements are not available.

The main contribution of this paper is to apply the DMD-KF to experimental flowfield and pressure sensor data generated by actuated airfoils at high angles of attack, an unsteady condition of interest for the application of feedback control. The first experiment, a pitching cambered ellipse, illustrates the selection of modes for the reduced-order model and shows the effect of the number of modes on the performance of the estimator. The second experiment, a surging NACA 0012, is evaluated to characterize the performance of the estimator for various flow conditions. Various sources of estimation error are analyzed and we suggest strategies to identify them.

The paper is organized as follows. Section II summarizes DMD, SPDMD, and DMD-KF. Section III describes the implementation of the SPDMD algorithm on two experimental data sets. It includes the experimental setups, and provides an overview of the process of selecting the number of DMD modes. Section IV evaluates the DMD-KF performance via comparison to the original and DMD reconstructed data. Section V summarizes the paper and ongoing work.

II. Data-driven model reduction and estimation

DMD is a data-driven algorithm to compute the eigenvalues and eigenmodes of a linear model that approximates the dynamics of data [16]. There are many variations of and additions to DMD [17]. This paper uses Schmid's algorithm [8] to obtain the DMD modes and eigenvalues and SPDMD by Jovanović, Schmid and Nichols [15] to select the most relevant modes for a reduced-order model. The Koopman Observer Form by Surana and Banaszuk [9] creates an observer matrix for the reduced-order model to be used in the DMD-KF for estimation [18].

A. Dynamic Mode Decomposition

Consider a dataset of $m+1$ snapshots, where each snapshot corresponds to a vector of observables $\boldsymbol{\psi}(t_k) \in \mathbb{R}^n$ at time step k for $k = 1, ..., m+1$. The time between steps must be constant, i.e., $t_{k+1} - t_k = \Delta t$. It is common for n (the dimension of the snapshot vector) to be much bigger than $m+1$ (the number of snapshots). For example, in fluids simulations or PIV data there are often more measurements than time steps. Form two matrices with these snapshots; the columns of these matrices contain the snapshot sequence, offset by one time step, such that

$$\Psi = \begin{bmatrix} | & | & & | \\ \boldsymbol{\psi}(t_1) & \boldsymbol{\psi}(t_2) & \cdots & \boldsymbol{\psi}(t_{m-1}) \\ | & | & & | \end{bmatrix} \quad \text{and} \quad \Psi' = \begin{bmatrix} | & | & | & \\ \boldsymbol{\psi}(t_2) & \boldsymbol{\psi}(t_3) & \cdots & \boldsymbol{\psi}(t_m) \\ | & | & | & \end{bmatrix}. \tag{1}$$

DMD yields an approximation of a linear operator A that advances the dynamics of the system one step forwards in time, i.e., $\Psi' = A\Psi$. The best fit for this operator can be found using the pseudoinverse †, so $A = \Psi'\Psi^\dagger$. However,

if $n \gg m$, this approach may not be practical. Instead, the eigenvalues and eigenvectors of A are obtained without computing A explicitly, using a projected version of A. Consider the Singular Value Decomposition (SVD)

$$\Psi = U\Sigma V^*, \tag{2}$$

where * indicates the conjugate transpose. The columns of U form the POD modes of the data set Ψ. The pseudoinverse of the SVD satisfies $\Psi^\dagger = V\Sigma^{-1}U^*$, which implies

$$A = \Psi' V\Sigma^{-1}U^*. \tag{3}$$

$\tilde{A}$ is a low-dimensional projection onto the POD basis [8] defined by the columns of U, i.e.,

$$\tilde{A} = U^*AU = U^*\Psi' V\Sigma^{-1}. \tag{4}$$

If $m < n$, computing the eigendecomposition of $\tilde{A}$ $(m \times m)$ is easier than computing the eigendecomposition of A $(n \times n)$. Let Λ be the diagonal matrix of eigenvalues of $\tilde{A}$ and W the matrix of right eigenvectors of $\tilde{A}$. The eigenvalues of A are the same as the eigenvalues of $\tilde{A}$ [19] and represent the DMD eigenvalues. The matrix of DMD modes

$$\Phi = UW \tag{5}$$

corresponds to the approximate eigenvectors of A [19]. Note that the DMD modes in (5) are a linear combination of POD modes.

Let the vector $\boldsymbol{\alpha}(t)$ of DMD mode amplitudes denote the approximate representation of the vector $\boldsymbol{\psi}(t)$ of observables in the DMD-mode basis, so $\boldsymbol{\psi}(t) \approx \Phi\boldsymbol{\alpha}(t)$. The time evolution is $\boldsymbol{\alpha}(t_{k+1}) = \Lambda\boldsymbol{\alpha}(t_k)$, which implies the approximate solution for the dynamics of the vector observable is [17]

$$\boldsymbol{\psi}(t) \approx \Phi\boldsymbol{\alpha}(t) = \Phi\Lambda^{(t-t_1)/\Delta t}\boldsymbol{\alpha}(t_1), \tag{6}$$

where $\Delta t = t_{k+1} - t_k$. using the decomposition (5) and (6) allows us to approximate the original data or data coming from the same dynamical system, but with different initial conditions . Note the DMD modes and eigenvalues are inherent to the dynamics, whereas the mode amplitudes depend on the initial conditions.

B. Sparsity Promoting Dynamic Mode Decomposition

DMD creates a sufficiently accurate reconstruction of data with only a few modes. To find those modes and their initial amplitudes, we employ the Sparsity Promoting DMD (SPDMD) algorithm developed by Jovanović [15], which consists of finding the mode amplitudes that minimize the cost function

$$J_\gamma\left(\boldsymbol{\alpha}(t_1)\right) = \sum_{k=1}^{m} ||\boldsymbol{\psi}(t_k) - \Phi\Lambda^{t_k/\Delta t}\boldsymbol{\alpha}(t_1)||^2 + \gamma|\alpha_k(t_1)|. \tag{7}$$

The first term in (7) corresponds to the difference between the original data and the DMD reconstruction, the second term is a penalty on non-zero mode amplitudes, and γ is a positive parameter that weights this penalty. After minimizing (7) for a particular value of γ, the modes with non-zero amplitudes are the modes chosen for the reconstruction; these modes correspond to the most influential modes. Then (7) is minimized again with $\gamma = 0$, using only the chosen modes, to obtain the optimal mode amplitudes to reconstruct the data with the reduced set of modes [15]. Although fewer modes yield a less accurate reconstruction, only a few modes may reproduce the dynamics of the system with a sufficient level of accuracy. The value of γ dictates the number m^* of chosen modes, so it represents the desired balance between the number of modes and the quality of the reproduction [15]. This process is illustrated in Section III.

C. Dynamic Mode Decomposition Kalman Filter

SPDMD is able to obtain the mode amplitudes that best fit a time series of training data. Determining the DMD mode amplitudes provides an estimate of the data, even in real time. A Kalman filter is a dynamic observer that gives real-time estimates of the system state given a dynamic model and noisy linear measurements from sensors. This section describes a method to estimate the mode amplitudes and thus the whole data set using only a subset of the measurements. Based on Surana's Koopman Observer Form [9], the main idea is to use DMD on the training data to generate a linear

dynamical system that represents the dynamics we observe and to use a Kalman Filter to estimate this system from sensor measurements in the test data.

When constructing the snapshot matrices from the training data, every snapshot $\boldsymbol{\psi}(t_k)$ must contain the states ($\boldsymbol{x} \in \mathbb{R}^{n_x}$) to be estimated concatenated together with the observables ($\boldsymbol{y} \in \mathbb{R}^{n_y}$) that will be readily available as measurements. Here, $\boldsymbol{x}$ corresponds to PIV measurements and $\boldsymbol{y}$ corresponds to pressure sensor measurements. The snapshot matrices are

$$\Psi = \begin{bmatrix} | & & | \\ \boldsymbol{x}(t_1) & \cdots & \boldsymbol{x}(t_m) \\ | & & | \\ - & - & - \\ | & & | \\ \boldsymbol{y}(t_1) & \cdots & \boldsymbol{y}(t_m) \\ | & & | \end{bmatrix} \qquad \Psi' = \begin{bmatrix} | & & | \\ \boldsymbol{x}(t_2) & \cdots & \boldsymbol{x}(t_{m+1}) \\ | & & | \\ - & - & - \\ | & & | \\ \boldsymbol{y}(t_2) & \cdots & \boldsymbol{y}(t_{m+1}) \\ | & & | \end{bmatrix}. \tag{8}$$

Next, apply the DMD and SPDMD algorithms to obtain a tuple of m^* DMD eigenvalues (λ_i) and DMD modes ($\boldsymbol{\phi}_i$) and arrange them so complex conjugates are grouped together. The amplitudes obtained from SPDMD are not required to create a DMD-based observer, however it is useful to have as reference the best possible reconstruction using the chosen set of modes. Form observation matrix C by letting C_i be the ith column of C with [9]

$$\begin{aligned} &C_i = \boldsymbol{\phi}_i \text{ if } \boldsymbol{\phi}_i \text{ is real, and} \\ &C_i = \mathrm{Re}\,(\boldsymbol{\phi}_i) \text{ and } C_{i+1} = \mathrm{Im}\,(\boldsymbol{\phi}_i) \text{ if } \boldsymbol{\phi}_i \text{ and } \boldsymbol{\phi}_{i+1} \text{ are complex conjugates.} \end{aligned} \tag{9}$$

Form the dynamics matrix F as a block diagonal matrix such that F has a diagonal entry $F_{i,i} = \lambda_i$, if λ_i is real, and block diagonal entry [9]

$$\begin{bmatrix} F_{i,i} & F_{i,i+1} \\ F_{i+1,i} & F_{i+1,i+1} \end{bmatrix} = \begin{bmatrix} \mathrm{Re}\,(\lambda_i) & \mathrm{Im}\,(\lambda_i) \\ -\mathrm{Im}\,(\lambda_i) & \mathrm{Re}\,(\lambda_i) \end{bmatrix}, \tag{10}$$

if λ_i and λ_{i+1} are complex conjugates. Split C into C_x and C_y, corresponding to the first n_x and the last n_y rows of C, respectively. Let z denote the vector of DMD amplitudes expressed in block modal form. These matrices define the linear dynamical system [9]

$$\boldsymbol{z}_k = F\boldsymbol{z}_{k-1} \tag{11a}$$
$$\boldsymbol{y}_k \approx C_y\boldsymbol{z}_k \tag{11b}$$
$$\boldsymbol{x}_k \approx C_x\boldsymbol{z}_k. \tag{11c}$$

If the system given by equations (11a) and (11b) is observable, then a linear state observer such as a Kalman filter will estimate $\boldsymbol{z}$ given measurements $\boldsymbol{y}$. The Kalman filter is the optimal algorithm to estimate the states of a linear system subject to Gaussian process noise with covariance Q and measurement noise with covariance R [18]. It involves propagating the current estimate $\hat{\boldsymbol{z}}$ and covariance P of the current estimate in time using knowledge of the dynamics and updating these values based on measurements. In this particular implementation, an extra step is added to compute the estimate of $\boldsymbol{x}$ using (11c). Given the system described by (11), the filter equations are [18]

$$\text{Estimate Propagation} \qquad \hat{\boldsymbol{z}}_k^- = F\hat{\boldsymbol{z}}_{k-1} \tag{12a}$$
$$P_k^- = FP_{k-1}F^T + Q \tag{12b}$$
$$\text{Kalman Gain} \qquad K_k = P_k^- C_y (C_y P_k^- C_y^T + R)^{-1} \tag{12c}$$
$$\text{Assimilating measurements} \qquad \hat{\boldsymbol{z}}_k = \hat{\boldsymbol{z}}_k^- + K(y_k - C_y\hat{\boldsymbol{z}}_k^-) \tag{12d}$$
$$P_k = (I - KC_y)P_k^- \tag{12e}$$
$$\text{Estimate of } \boldsymbol{x} \qquad \hat{\boldsymbol{x}}_k = C_x\hat{\boldsymbol{z}}_k. \tag{12f}$$

The superindex $^-$ refer to the estimate before assimilating measurements. The symbol $\hat{}$ indicates the quantity is an estimate, not the true value.

D. Sources of Error in the Dynamic Mode Decomposition Kalman Filter

The system dynamics (11) can be written as

$$\boldsymbol{x}_{k+1} = C_x F C_x^\dagger \boldsymbol{x}_k + \boldsymbol{w}_k; \qquad \boldsymbol{y}_k = C_y C_{\boldsymbol{x}}^\dagger \boldsymbol{x}_k + \boldsymbol{v}_k. \tag{13}$$

The process noise $\boldsymbol{w}_k$ and measurement noise $\boldsymbol{v}_k$ include the inherent noise from the dynamics and the loss of information due to the approximation. The process noise can be split into components either in, or orthogonal to, the span of DMD modes: i.e.,

$$\boldsymbol{w}_{k,\parallel} = C_x C_x^\dagger \boldsymbol{w}_k; \qquad \boldsymbol{w}_{k,\perp} = \boldsymbol{w}_k - \boldsymbol{w}_{k,\parallel}. \tag{14}$$

The terms $\boldsymbol{w}_{k,\parallel}$ and $\boldsymbol{v}_k$ correspond to the process and measurement noise in the reduced-order model and are related to the uncertainty induced by assuming a linear model for the reduced order dynamics. We compute Q and R as

$$Q = \mathrm{Cov}\left[C_x^\dagger x_{k+1} - F C_x^\dagger x_k\right]; \qquad R = \mathrm{Cov}\left[y_k - C_y C_x^\dagger x_k\right]. \tag{15}$$

In contrast, $\boldsymbol{w}_{k,\perp}$ is unrelated to the filtering process and corresponds to the inability of the chosen DMD modes to account for the variability in the states to be estimated. The DMD-KF will only produce estimates in the span of DMD modes, so the best possible estimate for the state, in the least squares sense, is $\tilde{\boldsymbol{x}} = C_x C_x^\dagger \boldsymbol{x}$. We denote this quantity as *DMD projection*. The DMD projection is useful to quantify the information lost from projecting into a low-dimensional model.

We distinguish between three different ways to recreate the evolution of a flowfield from a modal decomposition: projection, reconstruction, and estimation. Projection refers to projecting the test data into the span of the modes generated from the training data. This process yields the least possible ℓ_2 norm of the difference between instantaneous test data snapshot and a representation in terms of the selected modes, and thus can serve as a lower bound for the error. Reconstruction refers to finding the initial mode amplitudes that produce a trajectory, given by (6) (i.e., propagation of DMD modes assuming no process noise), which minimizes the difference from the test data. Estimation refers to the result of implementing a DMD-KF to obtain an approximation of the test data using only a limited set of measurements. A large difference between the projection and the reconstruction may indicate a large process noise covariance, which can be attributed to inherently noisy dynamics, or a flawed dynamic model. If the reconstruction error is small, but the estimation error is large, the problem may be due to a flawed measurement model.

III. Dynamic Mode Decomposition on an actuated airfoil

This section describes the application of the DMD and SPDMD procedures described in Sections II.A and II.B to two different experimental datasets from airfoils in periodic unsteady flow conditions. Both datasets consist of a time series of phase-averaged PIV data and pressure data from sensors embedded in the airfoils. Phase averaging means that several actuation cycles were done experimentally, then data corresponding to the same phase at different cycles was averaged together to produce a single cycle. This procedure reduces the noise in the data, but it also smooths out flow features that do not occur periodically. Getting rid of such features may or may not be desirable, but analyzing them is beyond the scope of this paper. We refer to these phase averaged datasets as the training datasets, as these are the sets from which the DMD modes for the DMD-KF are obtianed.

Experiment 1 consists of a pitching cambered ellipse in reverse flow, with 17 pressure sensors on the suction side of the airfoil and 13 pressure sensors on the high pressure side [20]. The states to estimate correspond to the velocity components at predetermined grid points in the airfoil frame of reference. Since the airfoil was pitching while the PIV cameras were stationary, the region around the airfoil where data could be gathered varied during the pitching cycle. DMD requires information about every state in every snapshot, so only the points for which there is data during the whole pitching cycle are included in the area of interest shown in Figure 2a, which is the largest area fixed in the body frame that remains in the field of view through a complete pitching cycle. Table 1 shows the parameters used in the experiments.

Parameter	Experiment 1 [20]	Experiment 2 [21]
Reynolds number	165000	40000
Free stream velocity	11.9 m/s	0.34m/s
Angle of attack	180°–200°	25°
Airfoil	Cambered ellipse	NACA 0012
Actuation	Pitching sinusoidally	Surging sinusoidally
PIV data points	16907	10369
Pressure sensors	30	8
Time steps	100	84–255

Table 1 Summary of experimental parameters.

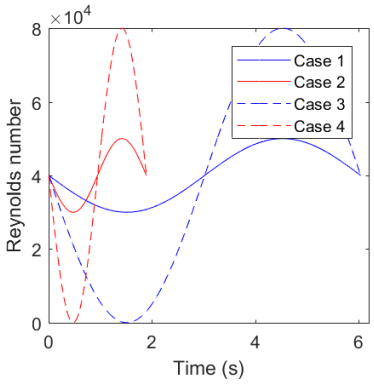

Fig. 1 Actuation trajectories for Experiment 2.

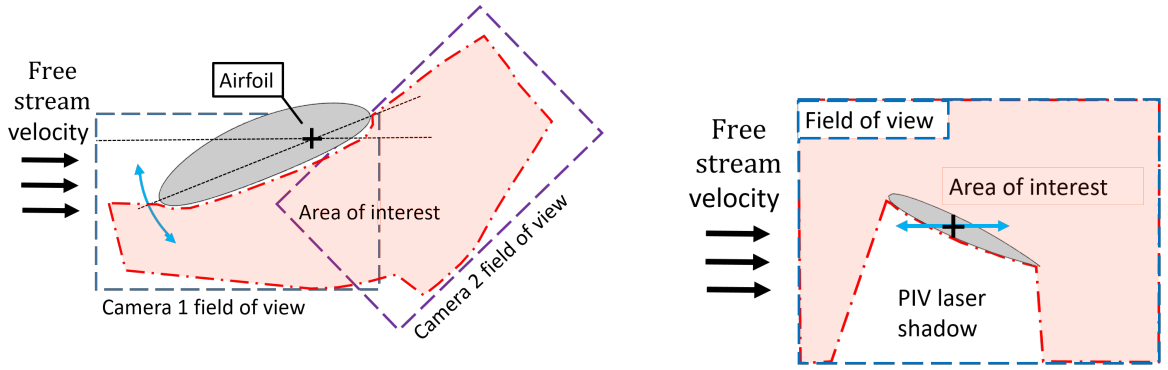

(a) Experiment 1 **(b) Experiment 2**

Fig. 2 Configuration of Experiments 1 and 2. a) Experiment 1: The area of interest is fixed in the airfoil frame [20]. b) Experiment 2: The camera moves with the airfoil so the area of interest is the field of view minus the airfoil and PIV shadow [21]. The teal arrows indicate the actuation direction.

Experiment 2 consists of a surging NACA 0012 airfoil with 8 pressure sensors on the suction side of the airfoil [21]. The Experiment 2 data set includes four different cases that vary the reduced frequency (k) and amplitude (Amp) of the surging motion, as shown in Figure 1. The amplitude is relative to the nominal Reynolds number and the reduced frequency is the actuation frequency ω nondimensionalized by the freestream velocity v_0 and the chord length c as

$$k = \frac{\omega c}{2v_0}. \tag{16}$$

The first step is to construct snapshot matrices as presented in (8), with $\boldsymbol{x}$ corresponding to PIV measurements arranged in a column vector and $\boldsymbol{y}$ corresponding to the pressure sensor data. The DMD modes and eigenvalues are obtained following the algorithm described in Section II.A. This algorithm produces m DMD modes, where $m+1$ is the number of time steps in the data, which is usually more than needed to accurately represent the system dynamics. Using fewer modes makes the estimation process run faster, so it is desirable to use only a small number of relevant modes. The SPDMD algorithm described in Section II.B is used for this purpose. Varying the sparsity promoting parameter γ provides a wide range of different mode numbers. Part of the SPDMD algorithm involves reconstructing the training data, which consists of finding the mode amplitudes that minimize the square of the difference between (6) evaluated at every time step and the original data. The reconstruction is important because it provides the best fit using (6) and thus can be used to evaluate if the system dynamics are well represented by a linear time evolution. The best number of modes can be chosen by looking at the percentage loss accuracy of the reconstruction (Figure 3b), or by plotting the reconstruction and comparing it qualitatively to the training data set (see Figure 4).

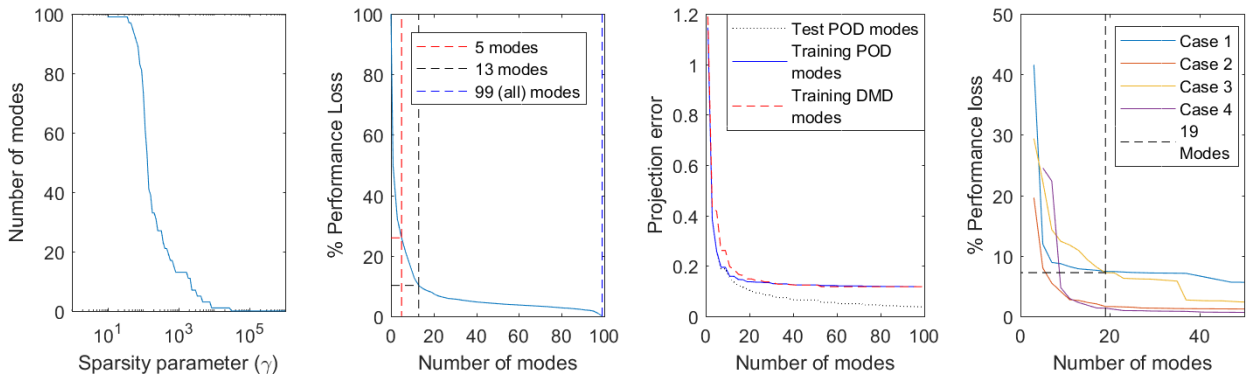

(a) Experiment 1 **(b) Experiment 1** **(c) Experiment 1** **(d) Experiment 2**

Fig. 3 (a) Number of modes chosen by SPDMD for different values of γ for Experiment 1. (b, d) Percent performance loss versus number of modes for Experiments 1 and 2. For Experiment 1: 5, 13 and 99 (all) modes are chosen for comparison. For Experiment 2: 19 modes are chosen for all cases. (c) Comparison of projection error for DMD and POD modes from the test set and POD modes from the training set for Experiment 1.

Figure 3a shows how the number of modes changes with γ in experiment 1. The percent performance loss from reconstruction of the data with DMD modes is defined as $100\sqrt{\frac{J_0(\alpha)}{J_0(0)}}$[15]. Figure 3b shows the percent loss of accuracy drops rapidly between 0 and 13 modes, which implies there are diminishing returns from using additional modes. Figure 4 shows the original data from Experiment 1 and the reconstruction at half the actuation period, when the leading edge vortex is about to be shed. The original data and the reconstruction with all the modes look nearly identical. In the reconstruction with 13 modes, the vortex can still be seen, but it is not as clearly defined. In the reconstruction with just five modes, the leading edge vortex does not appear; only the leading and trailing shear layers are visible.

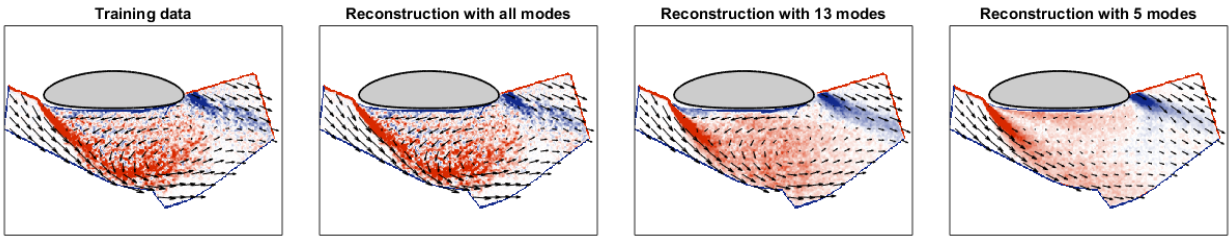

Fig. 4 Training set data and reconstructions with different number of modes for Experiment 1 at half the actuation period (t*=0.5). The reconstruction with all modes looks nearly identical to the original. With 13 modes some detail is lost but the main structures remain; with 5 modes the leading edge vortex indicated by the black box is not reproduced.

For estimation, the chosen modes are not used to represent the same data set from which the modes were obtained (the training set) but rather new data from the same dynamical system (the test set). To quantify the information lost from using a set of modes to represent a different realization of the system, we compute the projection of the test set into the span of the modes obtained from the training data. Fig. 3c shows the projection error using DMD and POD modes of the training set and POD modes of the test set for Experiment 1. Note that the test set consists of instantaneous PIV data, representative of a case of real-time estimation. POD modes form a more accurate projection of the data; the difference corresponds to using three or four more DMD modes for the same level of accuracy, similar to the result obtained in [2]. The projection error from the POD modes of the training and test data are very close for the first 10 modes, suggesting that they contain very similar information. For more modes obtained from the training set, the projection error stays almost constant. Even with the set of POD modes obtained from the test data, the projection error decreases slowly with the number of modes. Attaining an error below 5% requires over 60 POD modes.

IV. Dynamic Mode Decomposition Kalman Filter estimation results

After an appropriate number of modes is chosen, an observer is created following the procedure described in Section II.C. The DMD Kalman Filter estimates the mode amplitudes from pressure measurements in order to generate the corresponding estimate of the flowfield. For illustration purposes, we use Experiment 1 to show the results of choosing different numbers of modes and Experiment 2 to present results for different actuation cases. In both experiments, the DMD-KF is designed using phase-averaged data, but for Experiment 1, the estimation is tested using both phase averaged (from the training set) and instantaneous (from the test set) measurements. For Experiment 2, the test data consists of phase-averaged measurements, so only one period is available. The time t^* indicated in the results is the time normalized by the period of the actuation.

A. Experiment 1: Pitching cambered ellipse

We apply the DMD-KF to both the training and the test data to compare performance and identify if the model is overfitting the data. A plot of the estimation, reconstruction and projection error over a period is used to evaluate the estimator quantitatively. A plot of the flowfield is shown to identify if flow structures are being identified properly and to evaluate the performance of the estimator qualitatively.

Figures 5a to 5c show the normalized error the reconstruction, projection, and estimation of training data. The normalized error is defined as the average magnitude of the difference between the estimated (or reconstructed) field and the original flowfield, normalized by the average velocity during the period. At the initial time step, the reconstruction and estimation differ, but then quickly converge. The error in both the estimation and reconstruction with 5 modes rises around the middle of the period, which is consistent with the reconstruction being unable to properly reproduce the leading edge vortex that is shed around this time. The error also increases when using 13 modes but not as drastically as with 5 modes. The estimation using all modes takes more time to converge, and does not achieve the low error of the corresponding reconstruction using all the modes, but it does achieve the lowest error overall. A downside of using all modes is the increased computational time to compute the estimate, since the computational burden of computing a Kalman filter is highly dependent on the number of states [18].

Figures 5d to 5f show the corresponding normalized errors for the test data. Both the reconstruction and the estimation error increase, but the reconstruction error increased noticeably more. The reconstruction assumes no noise in the dynamics, so it is unable to correct for noisier dynamics and the difference in the evolution of the system between the test and the training data. The high value for the error in the case with 99 modes indicates that the extremely low value obtained in the reconstruction of training set data may be due to overfitting. When applied to the test data, the advantage of using more modes is lost. In fact, the reconstruction and estimation errors for 99 and 13 modes look nearly identical, which suggests that most modes beyond the first 13 are irrelevant for reproducing the dynamics of the new data set. It should also be noted that the estimation error approaches the projection error, so to improve the performance, it is necessary to find a set of modes that better account for the variation in the test data. As shown in Figure. 3c, many modes are needed to reduce the error significantly.

It is possible that the difference between the estimation and the test data is not a useful metric for the performance of the estimator. The test data contains turbulent flow, which might need to be filtered out to perform feedback control based on coherent flow structures. In this case, a new error metric should be developed, to quantify the filter's ability to identify flow features useful for feedback control. Motivated by this, the performance of the estimator is studied qualitatively. Figure 6 shows the results of implementing a DMD-KF choosing 13 modes for the estimation. For times $t^* = 0$ and $t^* = 0.2$, the estimation is able to reproduce the test data fairly accurately. For $t^* = 0.5$ the turbulent behaviour is not captured in detail, but the main flow features, such as the shear layers and the leading edge vortex, are present in the estimation.

B. Experiment 2: Surging NACA 0012

The DMD-KF was applied independently to four cases of Experiment 2, with the same number of modes, for comparison purposes. The number of modes $m^* = 19$ was chosen by looking at Figure 3d, which shows the percent performance loss versus number of modes. There is little improvement in performance by adding more than 19 modes in any of the cases. The estimation is performed on the same data from which the DMD modes are obtained, i.e., the training and the test data are the same.

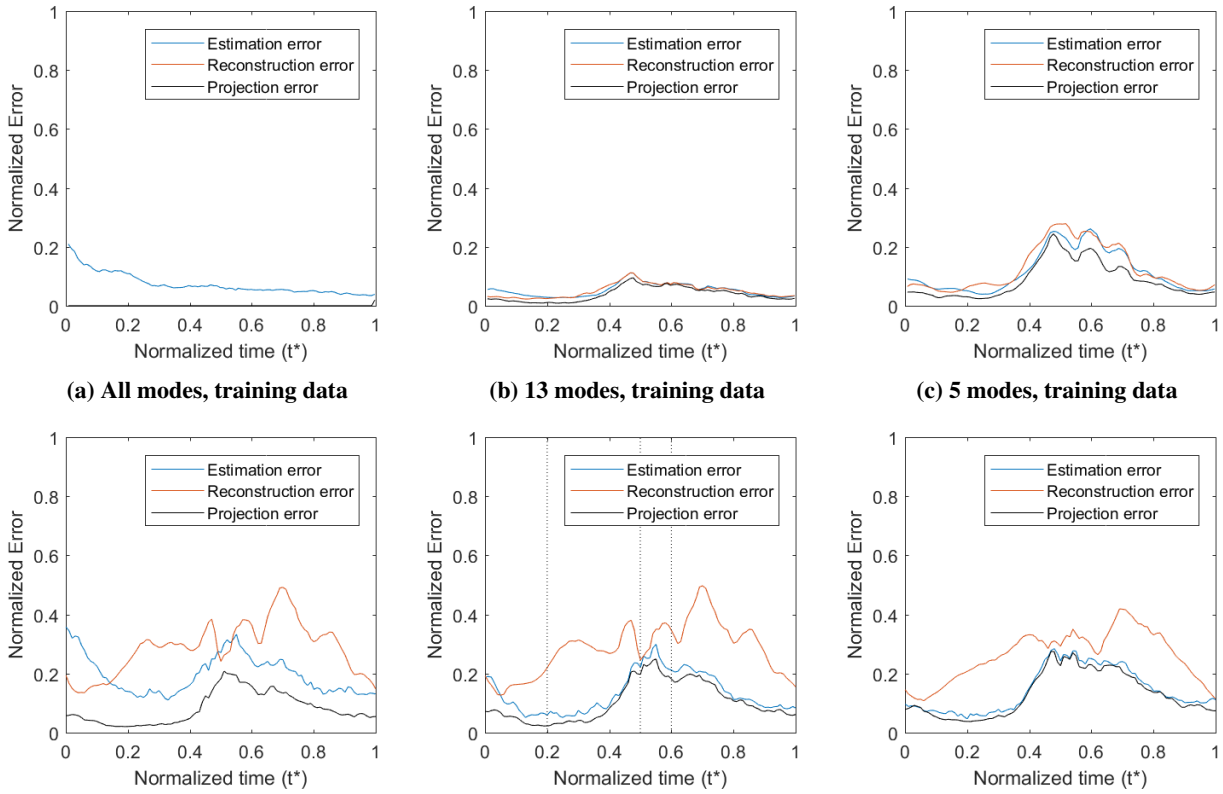

(a) All modes, training data **(b) 13 modes, training data** **(c) 5 modes, training data**

(d) All modes, test data **(e) 13 modes, test data** **(f) 5 modes, test data**

Fig. 5 Experiment 1: Estimation, reconstruction and projection error. The normalized error is the mean error in the velocity field, normalized by the average velocity. For estimation of the training data with all modes, error begins high but decreases consistently. In all other cases, the error increases near $t^* = 0.5$ due to inability to reproduce the highly turbulent separated flow. The vertical lines in (e) correspond to the frames shown in Figure 6.

Figure 7 shows the projection, reconstruction, and estimation error for all actuation cases in Experiment 2. In all cases, the initial estimation error was high. There are fewer sensors than modes, so the modes can not be inferred instantly, rather by comparing the predicted dynamics with the observations. The reconstruction error is also high at the initial time for most cases, while the projection error is low. It is possible that there are initial transients with a time evolution that is not well captured by the chosen modes. In the cases with $Amp = 1$; there is a secondary peak in estimation error; however in this case the reconstruction error is low. This result implies the system is evolving in a manner that is well approximated by the DMD linear model, but the DMD-KF is unable to capture the time evolution, possibly due to a flaw in the measurement model.

As a representative example, Figure 8 shows the flowfield for Case 3 at several points of interest. At the initial time there are large differences, especially around the tail of the airfoil. Around $t^* = 0.2$ the flow speed is low, which might mean the flow is hard to observe; there is a peak in error observed in Figure 7d. Around $t^* = 0.6$, the original and the estimation look nearly identical. During the remainder of the cycle, the shedding of the leading edge vortex occurs, a process with more turbulence, so it is expected that the error in both the estimate and the reconstruction will be higher. Nonetheless, it is possible to see on the frame corresponding to $t^* = 1$ that the estimate reproduces the main features in the flow.

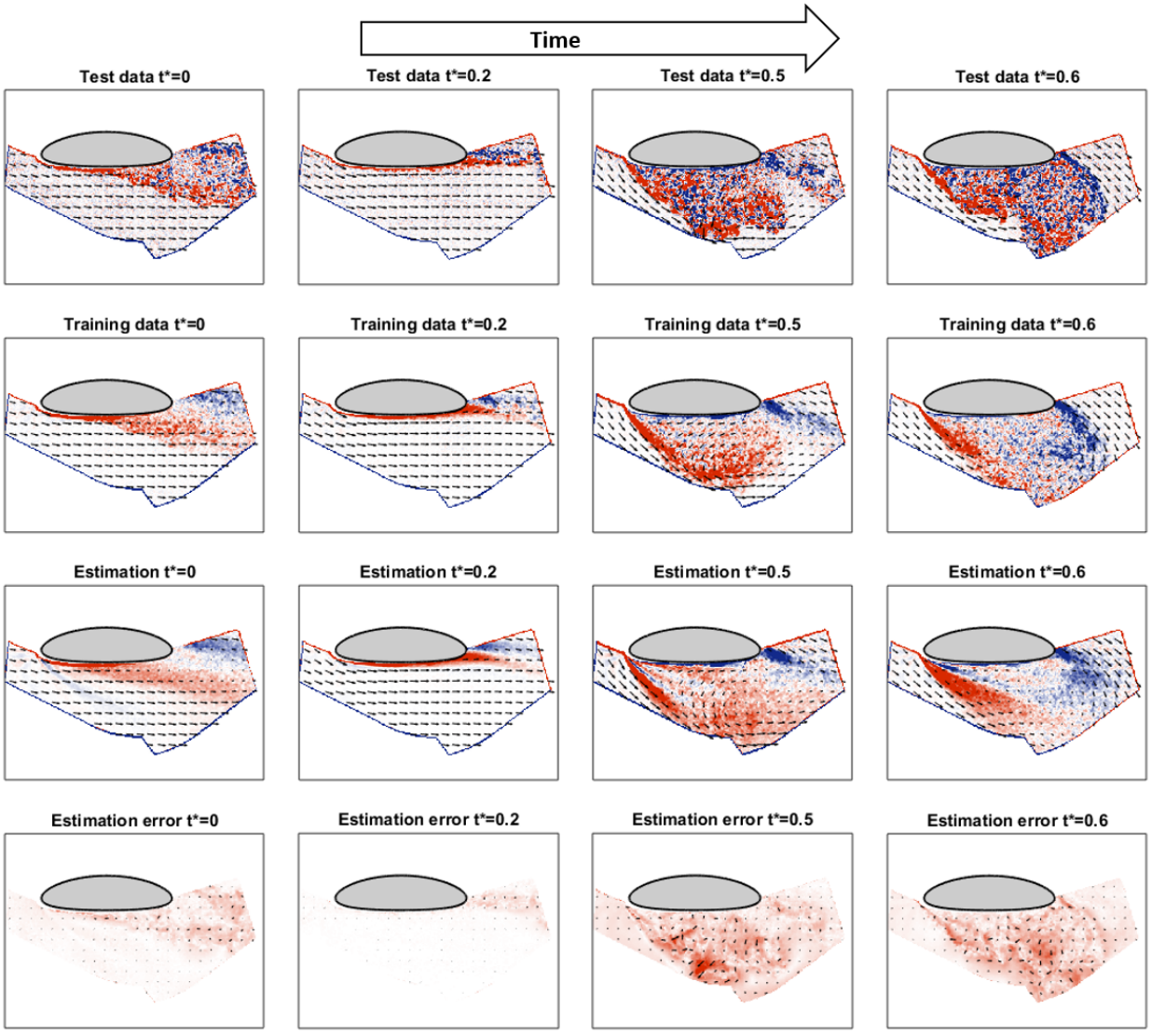

Fig. 6 Experiment 1: Test set data, training set data, and estimation of the test data with 13 modes at several times of interest. For $t^* = 0$ and $t^* = 0.2$, the estimation approximates the test data with very little error. For $t^* = 0.5$ and $t^* = 0.6$ there is more error overall, but the main flow structures, such as the shear layers and the leading edge vortex are reproduced.

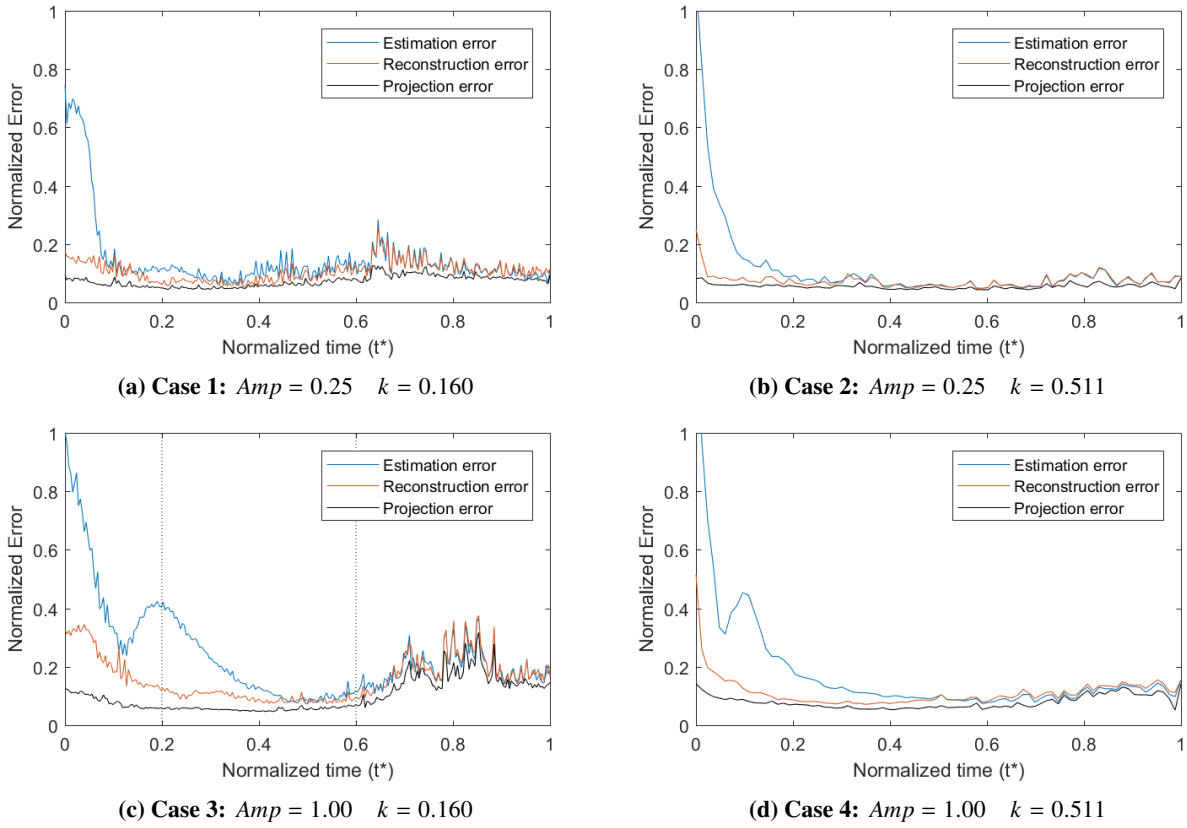

(a) Case 1: $Amp = 0.25 \quad k = 0.160$

(b) Case 2: $Amp = 0.25 \quad k = 0.511$

(c) Case 3: $Amp = 1.00 \quad k = 0.160$

(d) Case 4: $Amp = 1.00 \quad k = 0.511$

Fig. 7 Experiment 2: Estimation, reconstruction error and projection. Normalized error is as defined in figure 5. Initial error was consistently high but decreased rapidly. In some cases the estimation diverges from the reconstruction in the first half of the period, but in all cases they converge near the end. The vertical lines in Case 3 indicate the frames shown in Figure 8.

V. Conclusion

A Dynamic Mode Decomposition Kalman Filter (DMD-KF) was applied to estimate the unsteady flowfield around an actuated airfoil, using information from pressure sensors. This estimation method consists of using Sparsity Promoting Dynamic Mode Decomposition (SPDMD) [15] and the Koopan Observer Form [9] to create a linear system that approximates the dynamics of the unsteady flow, and a Kalman Filter to estimate the states in this linear system using pressure measurements.

The process of mode selection using SPDMD, and the effects of varying the number of modes, was shown using experimental results from a pitching cambered ellipse. There is a trade off with the number of modes: more modes increases the time for estimation convergence, both by increasing computational time and by taking more time steps to converge. In general, using more modes yields a better estimation, but using a small number of modes is enough to provide a fast and accurate representation of the flowfield.

The DMD reconstruction, DMD projection, and the DMD-KF estimation use DMD modes to approximate a flowfield. However the reconstruction and projection require complete knowledge of the flowfield to reproduce it with DMD modes, whereas the DMD-KF estimation uses pressure sensor measurements only. Estimation error may arise from the DMD modes not spanning the features of the data to estimate, or the dynamics may not be well approximated by a linear system. The DMD projection is useful to distinguish between both sources of error, since the projection is independent of the modeled dynamics.

Ogoing work is focused on using the DMD-KF flow estimation to obtain useful information, such lift or the position

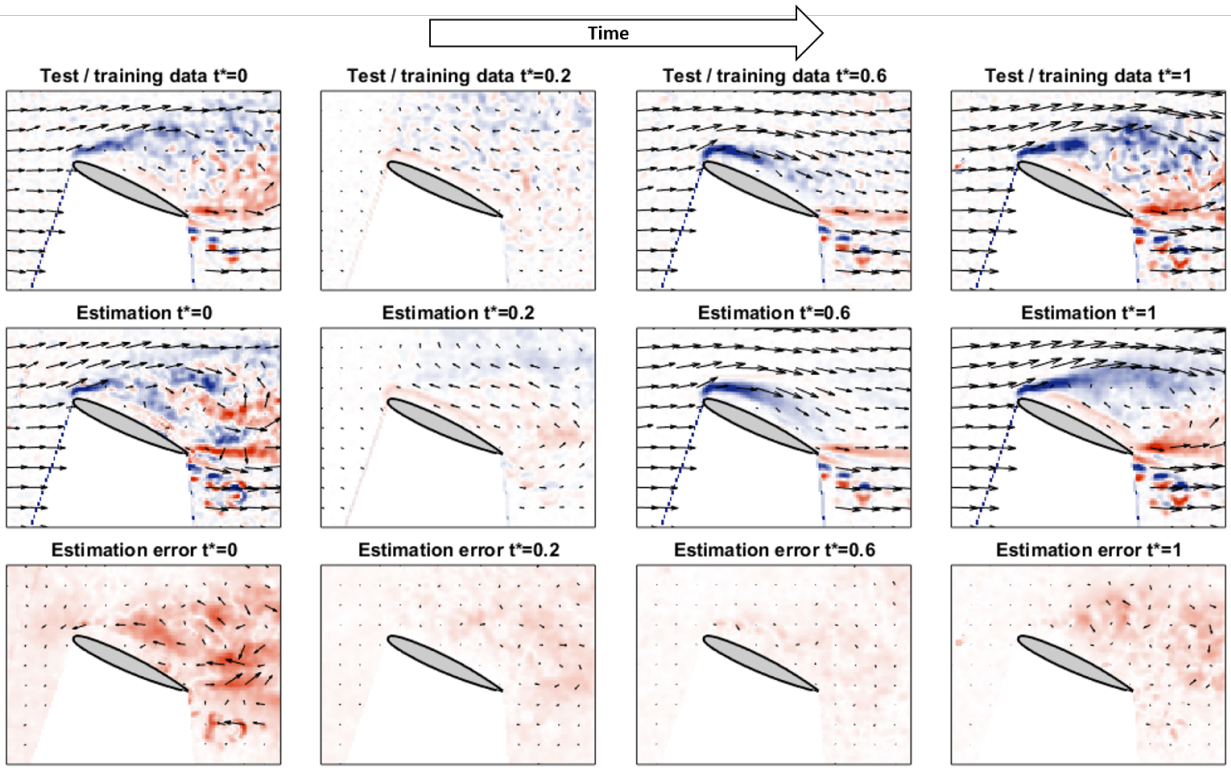

Fig. 8 Experiment 2: Original and estimated flowfield and estimation error using 19 modes at several times of interest for case 3. Error in estimation increases when the leading edge vortex is shed, but main features are still reproduced. For the original and estimation flowfields, the color red (blue) indicates positive (negative) vorticity. For the difference field, the color red indicates magnitude.

of the leading edge vortex, and evaluating the performance of the estimator in terms of these quantities. Note that the error measure presented in this paper is defined by comparing the velocity at every grid point, which does not necessarily reflect the quality of the estimation of specific flow features that may needed in practice for an effective feedback control.

Acknowledgments

Daniel F. Gomez thanks Jonathan Lefebvre for his help clarifying aerodynamic concepts and Girguis Sedky for his feedback on the preparation of this paper. This research was funded in part by AFOSR Grant No. FA95501810137. D. Gomez was supported by a Clark Doctoral Fellowship from the University of Maryland.

References

[1] Goman, M., and Khrabrov, A., "State-space representation of aerodynamic characteristics of an aircraft at high angles of attack," *Journal of Aircraft*, Vol. 31, No. 5, 1994, pp. 1109–1115. doi:10.2514/3.46618.

[2] Mariappan, S., Gardner, A. D., Richter, K., and Raffel, M., "Analysis of dynamic stall using Dynamic Mode Decomposition technique," *AIAA Journal*, Vol. 52, No. 11, 2014, pp. 2427–2439. doi:10.2514/1.J052858.

[3] Kim, J., and Bewley, T. R., "A Linear Systems Approach to Flow Control," *Annual Review of Fluid Mechanics*, Vol. 39, No. 1, 2007, pp. 383–417. doi:10.1146/annurev.fluid.39.050905.110153.

[4] Rowley, C. W., and Dawson, S. T., "Model Reduction for Flow Analysis and Control," *Annual Review of Fluid Mechanics*, Vol. 49, No. 1, 2017, pp. 387–417. doi:10.1146/annurev-fluid-010816-060042.

[5] Towne, A., Schmidt, O. T., and Colonius, T., "Spectral proper orthogonal decomposition and its relationship to dynamic mode decomposition and resolvent analysis," *Journal of Fluid Mechanics*, Vol. 847, 2018, p. 821–867. doi:10.1017/jfm.2018.283.

[6] Rowley, C. W., "Model feduction for fluids, using Balanced Proper Orthogonal Decomposition," *International Journal of Bifurcations and Chaos*, Vol. 15, No. 3, 2005, pp. 997–1013. doi:10.1142/S0218127405012429.

[7] Ahuja, S., and Rowley, C. W., "Feedback control of unstable steady states of flow past a flat plate using reduced-order estimators," *Journal of Fluid Mechanics*, Vol. 645, 2010, pp. 447–478. doi:10.1017/S0022112009992655.

[8] Schmid, P. J., "Dynamic mode decomposition of numerical and experimental data," *Journal of Fluid Mechanics*, Vol. 656, No. July 2010, 2010, pp. 5–28. doi:10.1017/S0022112010001217.

[9] Surana, A., and Banaszuk, A., "Linear observer synthesis for nonlinear systems using Koopman Operator framework," *IFAC-PapersOnLine*, Vol. 49, No. 18, 2016, pp. 716–723. doi:10.1016/j.ifacol.2016.10.250.

[10] Rowley, C. W., Mezi, I., Bagheri, S., Schlatter, P., and Henningson, D. S., "Spectral analysis of nonlinear flows," *Journal of Fluid Mechanics*, Vol. 641, 2009, pp. 115–127. doi:10.1017/S0022112009992059.

[11] Mezić, I., "Analysis of Fluid Flows via Spectral Properties of the Koopman Operator," *Annual Review of Fluid Mechanics*, Vol. 45, No. 1, 2013, pp. 357–378. doi:10.1146/annurev-fluid-011212-140652.

[12] Williams, M. O., Kevrekidis, I. G., and Rowley, C. W., "A data–driven approximation of the Koopman Operator: extending Dynamic Mode Decomposition," *Journal of Nonlinear Science*, Vol. 25, No. 6, 2015, pp. 1307–1346. doi:10.1007/s00332-015-9258-5.

[13] Hemati, M. S., Rowley, C. W., Deem, E. A., and Cattafesta, L. N., "De-biasing the dynamic mode decomposition for applied Koopman spectral analysis of noisy datasets," *Theoretical and Computational Fluid Dynamics*, Vol. 31, No. 4, 2017, pp. 349–368. doi:10.1007/s00162-017-0432-2.

[14] Dawson, S. T. M., Hemati, M. S., Williams, M. O., and Rowley, C. W., "Characterizing and correcting for the effect of sensor noise in the dynamic mode decomposition," *Experiments in Fluids*, Vol. 57, No. 3, 2016, pp. 1–19. doi:10.1007/s00348-016-2127-7.

[15] Jovanović, M. R., Schmid, P. J., and Nichols, J. W., "Sparsity-promoting Dynamic Mode Decomposition," *Physics of Fluids*, Vol. 26, No. 2, 2014, pp. 1–22. doi:10.1063/1.4863670.

[16] Chen, K. K., Tu, J. H., and Rowley, C. W., "Variants of Dynamic Mode Decomposition: Boundary Condition, Koopman, and Fourier Analyses," *Journal of Nonlinear Science*, Vol. 22, No. 6, 2012, pp. 887–915. doi:10.1007/s00332-012-9130-9.

[17] Nathan Kutz, J., Brunton, S., Brunton, B., and L. Proctor, J., *Dynamic Mode Decomposition: Data-Driven Modeling of Complex Systems*, SIAM, 2016. doi:10.1137/1.9781611974508.

[18] Crassidis, J. L., and Junkins, J. L., *Optimal Estimation of Dynamic Systems, Second Edition (Chapman & Hall/CRC Applied Mathematics & Nonlinear Science)*, 2nd ed., Chapman & Hall/CRC, 2011.

[19] Tu, J. H., Rowley, C. W., Luchtenburg, D. M., Brunton, S. L., and Kutz, J. N., "On Dynamic Mode Decomposition - theory and applications," Ph.D. thesis, Princeton, 2013. doi:10.3934/jcd.2014.1.391.

[20] Lind, A. H., "An Experimental Study of Static and Oscillating Rotor Blade Sections in Reverse Flow," Ph.D. thesis, University of Maryland, 2015. doi:10.13016/M22M8H.

[21] Kirk, P. B., and Jones, A. R., "Vortex formation on surging aerofoils with application to reverse flow modelling," *Journal of Fluid Mechanics*, Vol. 859, 2019, p. 59–88. doi:10.1017/jfm.2018.800.